

**Finger properties in bounded double diffusive finger convection**A. Rosenthal<sup>1</sup> and A. Tilgner<sup>1, a)</sup>*Institute of Astrophysics and Geophysics, University of Göttingen,  
Friedrich-Hund-Platz 1, 37077 Göttingen, Germany*

(Dated: February 19, 2025)

We analyze experimental data on double diffusive convection in an electrochemical cell in the finger regime. All fingers in the experiments are bounded on at least one end by a solid wall. The properties of these fingers are compared with those of fingers in other experiments which are surrounded by fluid on all sides. The compositional boundary layers are found to be thinner than the finger width. The finger thickness agrees well with half the wavelength of the fastest growing mode obtained in linear stability analysis. The ion transport through the boundary layers is reduced by two orders of magnitude compared with unbounded fingers. The overturning layers in staircases contribute negligibly to salinity mixing because of efficient transport between finger layers and convection rolls.

arXiv:2502.12792v1 [physics.flu-dyn] 18 Feb 2025

---

<sup>a)</sup>corresponding author: andreas.tilgner@phys.uni-goettingen.de

## I. INTRODUCTION

Double diffusive convection occurs if the density of a fluid is governed by two different properties with different diffusion rates, such as temperature and salinity in ocean water. Ocean water is the paradigmatic example of a fluid prone to double diffusive effects, but many other examples exist for this phenomenon<sup>1-3</sup>. The behaviour of double diffusive convection very much depends on which property acts to destabilize the fluid. In this paper, we will be concerned with the case in which the rapidly diffusing component (temperature in the example of sea water) on its own leads to a stable stratification of the medium while the slowly diffusing property (salinity in the case of sea water) drives an overturning motion. This combination of temperature and salinity gradients may lead to finger convection in which the convection cells take the form of slender cells elongated along the vertical. Depending on control parameters, these fingers occupy the entire fluid volume or they occur in vertically stacked layers separated by layers filled with wide convection rolls familiar from simple Rayleigh-Bénard convection. Flows of the second kind are called staircases.

This type of convection already was the topic of numerous numerical and experimental studies<sup>3</sup>. The experiments<sup>4</sup> are limited in the parameter range they can explore by the available fluids and the size of the apparatus. They also face the challenge of maintaining a sufficiently constant salinity gradient. Most experiments actually investigate non stationary conditions in which an initial salinity gradient or a salinity difference between two layers is eroded in the course of time due to convection. In these systems, fingers are similar to fingers in an unbounded domain in that they end within the fluid domain and are surrounded by fluid from all sides. Those experiments that maintain truly stationary conditions<sup>5-7</sup> generate fingers at least some of which are limited in their vertical extent by solid boundaries. Most numerical simulations also investigated unbounded fingers and only few numerical studies of bounded fingers at high Rayleigh numbers exist<sup>8-11</sup>.

The present paper analyzes data obtained from experiments on double diffusive electrochemical convection. As opposed to other applications of electrochemical convection<sup>12</sup>, care was taken to eliminate the effects of electrical fields so that the dynamics are solely determined by advection and diffusion. The important characteristics of this experiment in comparison with other double diffusive systems is that the system can be maintained in a steady state and the control parameters describing material properties are large. The

Prandtl and Schmidt numbers (to be defined below, and see table I for a summary of the nomenclature) are around 9 and 2000, respectively, whereas they are 7 and 700 for sea water. The fingers observed in the experiments analyzed here have at least one tip bordering a solid plate, so that the effect of a solid boundary can be investigated through comparison with results on unbounded fingers.

The next section reviews the experimental procedures. Previous publications on double diffusive electrochemical convection<sup>7,13,14</sup> focused on transitions between different flow regimes which could not be mapped out in other experiments. The aim of the present paper is to connect observations on finger properties in double diffusive electrochemical convection with analogous results on different double diffusive systems. These concern the finger thickness in the next section, and the salinity transport through finger layers and staircases in sections IV and V, respectively.

## II. THE EXPERIMENT

The electrochemical system under study sketched in Fig. 1 is introduced in detail in Ref. 15 and its use for double diffusive convection is explained in Refs. 7, 13, and 14 so that only a brief summary of the technique is presented here. The convecting fluid is a solution of cupric sulfate in sulfuric acid contained in a cell with top and bottom boundaries made of copper. These two boundaries are regulated in temperature to maintain a temperature difference from top to bottom. In addition, a voltage is applied to the two boundaries which then act as electrodes with copper ions detaching at the top and reattaching at the bottom boundary. The ions of the acid do not participate in the electrochemistry and accumulate in microscopic layers next to the boundaries so that the bulk of the cell is free of electric fields and the copper ions diffuse and are advected the same as salinity in other double diffusive systems.

Four control parameters describe the system within the Boussinesq approximation. The Prandtl and Schmidt numbers,  $Pr$  and  $Sc$ , are defined as

$$Pr = \frac{\nu}{\kappa} \quad , \quad Sc = \frac{\nu}{D}, \quad (1)$$

with  $\nu$  the kinematic viscosity,  $\kappa$  the thermal diffusivity, and  $D$  the diffusion constant of copper ions. The other two control parameters are the thermal and chemical Rayleigh

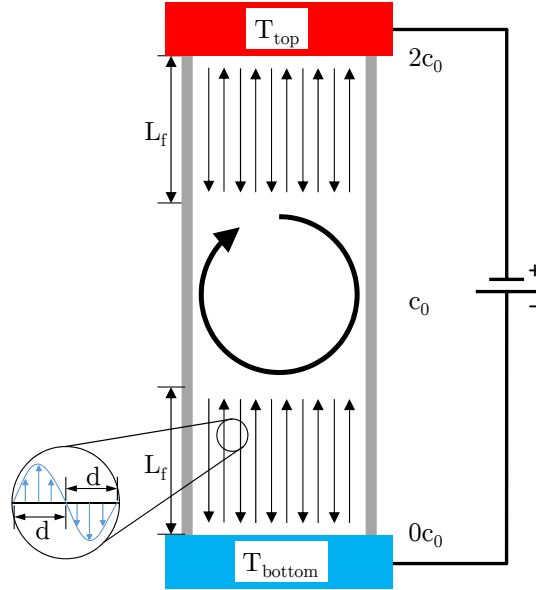


Figure 1. Sketch of the experiment. Two copper electrodes are regulated in temperature, the upper electrode is heated while the lower electrode is cooled. The average concentration of copper ions in the electrolyte is  $c_0$ . An applied voltage drives the limiting current through the electrolyte so that the copper concentration is zero at the bottom electrode and  $2c_0$  at the top electrode. Fingers of thickness  $d$  either cross the entire cell or (as sketched in this figure) they are part of a staircase in which case they fill two layers of height  $L_f$  each with a layer with overturning motion in between the two finger layers. The velocity field within fingers is symbolically sketched in the magnified excerpt.

numbers,  $Ra_T$  and  $Ra_c$ , given by

$$Ra_T = \frac{g\alpha\Delta TL^3}{\kappa\nu} \quad , \quad Ra_c = \frac{g\beta\Delta cL^3}{D\nu} \quad , \quad (2)$$

where  $g$  is the gravitational acceleration,  $L$  is the height of the cell,  $\alpha$  and  $\beta$  are the thermal and compositional expansion coefficients, and  $\Delta T$  and  $\Delta c$  are the temperature and copper ion concentration differences between top and bottom. The sign convention is chosen such that  $\alpha$  and  $\beta$  are positive and

$$\Delta T = T_{\text{bottom}} - T_{\text{top}} \quad , \quad \Delta c = c_{\text{top}} - c_{\text{bottom}} \quad (3)$$

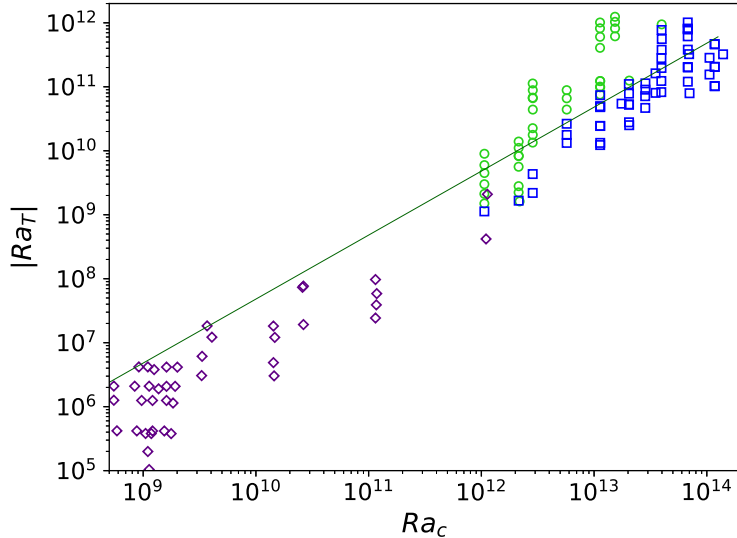


Figure 2. Overview of the available experimental data in the  $(Ra_c, Ra_T)$ -plane. Circles and diamonds represent states with fingers crossing the entire cell from top to bottom whereas squares are staircases. The straight line indicates  $|\Lambda| = 1$ .

so that positive Rayleigh numbers correspond to unstable and negative Rayleigh numbers to stable stratification.

The Prandtl and Schmidt numbers are essentially fixed in our experiments at  $Pr \approx 9$  and  $Sc \approx 2000$ . The Rayleigh numbers on the other hand can be varied, most efficiently by using cells of different heights. Values for  $L$  of  $2cm$ ,  $4cm$ ,  $8cm$ ,  $20cm$ ,  $40cm$  and  $80cm$  appear in our data set. The  $\Delta T$  in  $Ra_T$  is conveniently adjusted through the temperature control of the electrodes, while  $\Delta c$  in  $Ra_c$  is varied by using solutions of different copper concentration (or "salinity")  $c_0$ . The cell is always operated at the limiting current<sup>7,15</sup> which implies that  $\Delta c = 2c_0$ .

It will sometimes be useful to replace one of the Rayleigh numbers by another control parameter which is the density ratio  $\Lambda$  given by

$$\Lambda = \frac{Ra_T}{Ra_c} \frac{Sc}{Pr} = \frac{\alpha \Delta T}{\beta \Delta c}. \quad (4)$$

The data analyzed in this paper is taken from the experiments described in Refs. 7 and 14. The Rayleigh numbers of the available data are shown in Fig. 2. The data points are split into three classes in this figure: They are either taken from Ref. 7 (indicated by diamonds) and correspond to flow states with fingers extending from one boundary to the

other at  $Ra_c$  small enough (except for two points) so that staircases do not appear at any  $|Ra_T|$  for this  $Ra_c$ , or to flow states also with fingers crossing the entire cell but at  $Ra_c$  large enough so that staircases form at suitable  $|Ra_T|$  (circles in Fig. 2), and finally the staircases themselves in which the fingers are interrupted by a convection roll (shown by squares). These symbols will be used again in the subsequent figures because it facilitates their reading and conveniently identifies the origin of the data points. A few crude features are associated with the different types of points. The diamonds are flow states with very regular fingers and nearly all these points have  $|\Lambda| < 1$ . The data collected at these Rayleigh numbers obey simple scaling laws<sup>7</sup>. The circles correspond to more diverse flow states<sup>14</sup>. The fingers at high  $Ra_c$  are more time dependent and disordered, sometimes with finger widths varying as a function of height. The staircases all have the same structure: They consist of a top and bottom finger layer with an intervening overturning layer. No staircases with fewer or more layers appear in the data set.

The most obvious measurement collected from the experiments is the Sherwood number  $Sh$  which quantifies the ion flux through the layer and which is defined as

$$Sh = \frac{j L}{z F D \Delta c} \quad (5)$$

if  $j$  is the current density,  $z$  the valence of the ion ( $z = 2$  for  $Cu^{2+}$ ), and  $F$  is Faraday's constant. Sherwood number is the usual designation for the non dimensional form of the ion flux through the cell within the electrochemical literature, whereas it is typically called the chemical Nusselt number or the salinity Nusselt number in the literature dedicated to double diffusion.

The velocity field is obtained from particle image velocimetry (PIV) in a vertical plane near the center of the cell. PIV allows us to determine one horizontal component of velocity  $v_x$  together with the vertical component  $v_z$ . An average velocity  $v$  is then computed as

$$v = \left( \frac{1}{A} \int \langle v_x^2 + v_z^2 \rangle dA \right)^{1/2} \quad (6)$$

where the integral extends over the area  $A$  of the vertical plane containing fingers. This is the area of the entire plane illuminated for PIV in the case of fingers crossing the whole cell, but it excludes the area filled by wide convection rolls in staircases. The angular brackets denote average over time. The velocity  $v$  is then used to compute a global Reynolds number  $Re$ , and when dealing with staircases, it is also useful to define a Reynolds number on the

scale of the finger height  $L_f$ :

$$Re = \frac{vL}{\nu} \quad , \quad Re_f = \frac{vL_f}{\nu}. \quad (7)$$

The thickness of the finger layers  $L_f$  is extracted from the velocity fields obtained by PIV<sup>14</sup>. One would also like to attribute Rayleigh numbers to finger layers within staircases, but we do not know the concentration and temperature differences between the top and bottom of these layers. Let us first define the Rayleigh numbers  $Ra_{T,f}$  and  $Ra_{c,f}$  of finger layers as

$$Ra_{T,f} = \frac{g\alpha\Delta T_f L_f^3}{\kappa\nu} \quad , \quad Ra_{c,f} = \frac{g\beta\Delta c_f L_f^3}{D\nu}. \quad (8)$$

It will be argued below that the following definitions for  $\Delta T_f$ ,  $\Delta c_f$  and also  $L_f$  are reasonable in figures showing data for both staircases and fingers crossing the whole cell: If fingers extend from one boundary to the other, then one obviously selects  $L_f = L$ ,  $\Delta T_f = \Delta T$  and  $\Delta c_f = \Delta c$ . For finger layers in staircases (which all contain two finger layers in our data base),  $L_f$  is the layer depth,  $\Delta T_f = \Delta T/2$  and  $\Delta c_f = \Delta c$ . This last definition of  $\Delta c_f$  is different from the one used in Ref. 14. Section V will explain why this modification is necessary.

There is a characteristic length scale that can be extracted from the PIV measurements and that we will identify with a finger thickness. It is straightforward to determine a reasonable finger thickness for the very regular time independent flows at low  $Ra_c$ , but a more refined treatment is necessary at high  $Ra_c$ . A definitive characterization of finger shape requires 3D velocity fields which are not available. Hage and Tilgner<sup>7</sup> concluded from the combination of PIV and Sherwood number measurements that the fingers are lamellar rather than tubular. Different orientations of the lamellae with respect to the plane of illumination of the PIV lead to different apparent finger thicknesses. The minimal thickness is observed if lamellae and plane of illumination are orthogonal to each other, and the thickness measured in this geometry is what one would call finger thickness if horizontal cross sections of the velocity field were available. However, one has to find a compromise between the search for a minimum and the need for noise reduction through averaging, so that we opted for the following procedure: First, count in every instantaneous velocity field obtained from PIV the number of zero crossings of  $v_z$  as a function of the horizontal coordinate  $x$  and deduce an average separation of zeros of  $v_z$  at every height  $z$ . Then, select the height at which this average is minimal. This is also done with flow states in mind which are near the transition

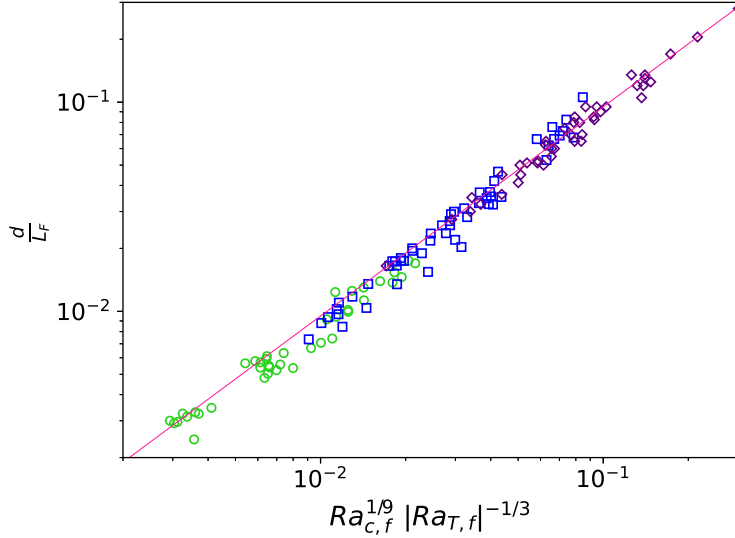


Figure 3. The finger width  $d$  divided by the finger height  $L_f$  as a function of  $|Ra_{T,f}|^{-1/3} Ra_{c,f}^{1/9}$  to verify eq. (9) which is represented by the continuous line. The symbols are the same as in fig. 2.

form pure finger convection to staircases. When a central layer with a broad convection cell develops, the fingers widen near the interface to the convection roll<sup>14</sup>, and we assume the finger size far away from that interface to be the relevant finger size. Finally, the minimal thickness thus obtained in every instantaneous velocity field is averaged over time. This yields the length  $d$  which we use for finger thickness in the data analysis below.

### III. FINGER THICKNESS

The finger thickness is a quantity that received much interest from both numerical simulations and experiments because there is a simple hypothesis to test: It is tempting to assume that for any given stratification, the finger mode with the fastest growth rate according to linear stability analysis contains fingers of the size that will be observed in the saturated non linear state. This section will compare the experimentally obtained finger thickness with the predictions deduced from this assumption.

The experiments on the regular fingers at low  $Ra_c$  obey a simple scaling law<sup>7</sup>. If we generalize the variables to include fingers in staircases, this scaling law is

$$\frac{d}{L_f} = 0.95 |Ra_{T,f}|^{-1/3} Ra_{c,f}^{1/9}. \quad (9)$$

As Fig. 3 shows, this relation fits very well all types of fingers, which corroborates the

scaling law, but also the procedure to determine finger widths and the definitions of  $Ra_{T,f}$  and  $Ra_{c,f}$ . However, the relation with fastest growing modes is not apparent.

The equations of evolution for the fields of velocity  $\mathbf{v}(\mathbf{r}, t)$ , temperature  $T(\mathbf{r}, t)$ , salinity or concentration  $c(\mathbf{r}, t)$  and pressure  $p(\mathbf{r}, t)$  are given by

$$\partial_t \mathbf{v} + (\mathbf{v} \cdot \nabla) \mathbf{v} = -\frac{1}{\rho} \nabla p + \nu \nabla^2 \mathbf{v} + g\alpha T \hat{\mathbf{z}} - g\beta c \hat{\mathbf{z}} \quad (10)$$

$$\nabla \cdot \mathbf{v} = 0 \quad (11)$$

$$\partial_t T + \mathbf{v} \cdot \nabla T = \kappa \nabla^2 T \quad (12)$$

$$\partial_t c + \mathbf{v} \cdot \nabla c = D \nabla^2 c \quad (13)$$

where  $\hat{\mathbf{z}}$  denotes a unit vector in the vertical direction,  $\rho$  is the density and the other variables have the meaning assigned to them in the previous section. The lower and upper boundaries are represented by the conditions that  $\mathbf{v} = 0$  and that  $T$  and  $c$  have prescribed fixed values on the boundaries. However, theoretical analysis is easiest in an infinitely extended domain. We therefore split  $T$  and  $c$  into horizontal and temporal averages  $\bar{T}$  and  $\bar{c}$  and fluctuations  $\theta$  and  $s$  around that mean:

$$T(\mathbf{r}, t) = \bar{T}(z) + \theta(\mathbf{r}, t) \quad (14)$$

$$c(\mathbf{r}, t) = \bar{c}(z) + s(\mathbf{r}, t). \quad (15)$$

In a plane layer with  $T$  and  $c$  imposed on horizontal boundaries,  $\bar{T}$  and  $\bar{c}$  are a priori unknown and have to be determined as part of the solution, whereas they are imposed as the driving agent in models in infinitely extended volumes, in which case it is convenient to choose  $\bar{T}$  and  $\bar{c}$  such that their gradients are constant.

The equations (10-13) linearized around  $v_z = 0$ ,  $\theta = 0$  and  $s = 0$  become

$$\partial_t v_z = -\frac{1}{\rho} \partial_z p + \nu \nabla^2 v_z + g\alpha \theta - g\beta s \quad (16)$$

$$\partial_t \theta + v_z \partial_z \bar{T} = \kappa \nabla^2 \theta \quad (17)$$

$$\partial_t s + v_z \partial_z \bar{c} = D \nabla^2 s. \quad (18)$$

These equations are solved in an infinite domain with constant  $\partial_z \bar{T}$  and  $\partial_z \bar{c}$  by solutions of the form  $(v_z, \theta, s) = (v_0, \theta_0, s_0) e^{\sigma t} e^{i(k_x x + k_y y)}$  to yield a growth rate  $\sigma$  as a function of wavenumber  $k = \sqrt{k_x^2 + k_y^2}$ . One can then determine the wavenumber  $K$  at which  $\sigma$  is maximum. The result of this computation is well known<sup>16,17</sup> and is sometimes summarized

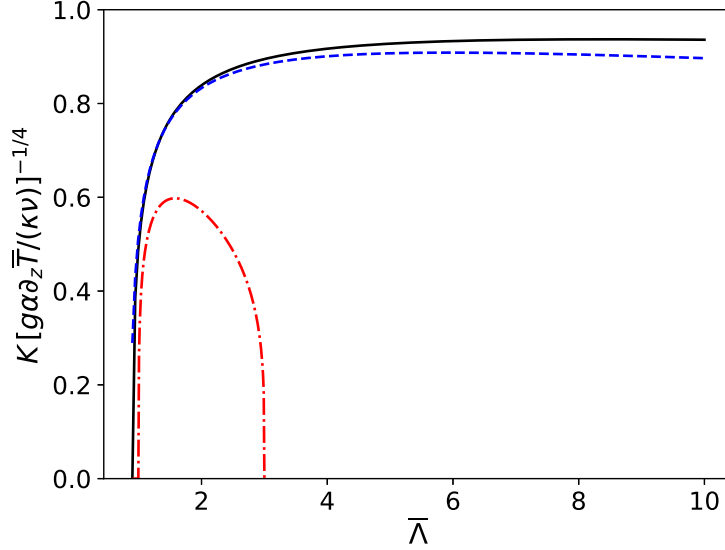


Figure 4.  $K[g\alpha\partial_z\bar{T}/(\kappa\nu)]^{-1/4}$  as a function of  $\bar{\Lambda}$  for the electrolyte investigated in this paper ( $Pr = 9$ ,  $Sc = 2000$ , black continuous line), sea water ( $Pr = 7$ ,  $Sc = 700$ , blue dashed line) and salt and sugar in aqueous solution ( $Pr = 700$ ,  $Sc = 2100$ , red dot dashed line).

as  $K[g\alpha\partial_z\bar{T}/(\kappa\nu)]^{-1/4} = \text{const.}$  However, there is also a dependence on  $Pr$  and  $Sc$  and also the density ratio which in the unbounded model is best defined as

$$\bar{\Lambda} = \frac{\alpha\partial_z\bar{T}}{\beta\partial_z\bar{c}}. \quad (19)$$

There are no growing modes for  $\bar{\Lambda} > Sc/Pr$ . One naively expects that narrow finger modes are replaced by overturning motion of arbitrarily long wavelength for  $\bar{\Lambda} < 1$ , but this is not strictly true as finger modes also exist for  $\bar{\Lambda}$  slightly below 1 for the  $Sc$  and  $Pr$  of interest to laboratory experiments<sup>17</sup>. Fig. 4 shows  $K[g\alpha\partial_z\bar{T}/(\kappa\nu)]^{-1/4}$  as a function of  $\bar{\Lambda}$  for the most common laboratory fluids. One recognizes that for cupric sulfate in sulfuric acid and for sea water, the product  $K[g\alpha\partial_z\bar{T}/(\kappa\nu)]^{-1/4}$  is close to 0.9 for a wide range of  $\bar{\Lambda}$ .

We do not know from measurements the correct value of  $\partial_z\bar{T}$  within the electrochemical cell. As a first guess, let us assume that  $\partial_z\bar{T} = -\Delta T/L$ . The wavenumber  $K$  corresponds to  $\pi/d$ , so that  $K[g\alpha\partial_z\bar{T}/(\kappa\nu)]^{-1/4} = \pi L/d|Ra_T|^{-1/4}$ , which is shown in in Fig. 5 as a function of  $|\Lambda|$ . The points scatter around 1.1 rather than 0.9, but apart from this 20% discrepancy, the fastest growing mode assuming an interior temperature gradient of  $-\Delta T/L$  is a good prediction for the actual finger thickness.

We will now discuss by how much the true value of  $\partial_z\bar{T}$  can depart from  $-\Delta T/L$ . To

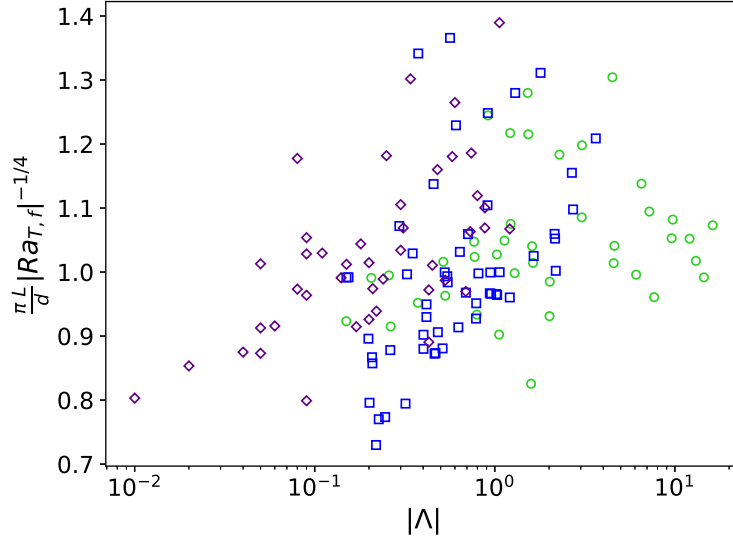


Figure 5.  $\frac{\pi L}{d} |Ra_{T,f}|^{-1/4}$  as a function of  $|\Lambda|$ . The symbols are the same as in fig. 2.

this end, we first relate the fluctuations  $\theta$  to the mean  $\bar{T}$  by

$$v_z \partial_z \bar{T} = \kappa (\partial_x^2 + \partial_y^2) \theta. \quad (20)$$

This equation describes an elevator mode and follows from eq. (12) if the flow is stationary, if  $|v_x| \ll |v_z|$  (which is satisfied because of the large anisotropy of velocity within the fingers<sup>13</sup>), and if  $\theta$  does not depend on  $z$ . Let us check the self consistency of this last assumption. Eq. (20) admits solutions of the form  $v_z = v_0 \cos(\pi x/d)$  and  $\theta = -\frac{v_0 d^2}{\pi^2 \kappa} \partial_z \bar{T} \cos(\pi x/d)$  if  $\partial_z \bar{T}$  is constant, so that the total temperature

$$T = z \partial_z \bar{T} + \theta = \partial_z \bar{T} \left[ z - \frac{v_0 d^2}{\pi^2 \kappa} \partial_z \bar{T} \cos\left(\frac{\pi x}{d}\right) \right] \quad (21)$$

is constant on  $z - \frac{v_0 d^2}{\pi^2 \kappa} \cos(\pi x/d) = \text{const}$ . Isotherms are thus sinusoids with amplitudes  $\Delta z$  given by

$$\frac{\Delta z}{L} = \frac{1}{\sqrt{2} \pi^2} \left( \frac{d}{L} \right)^2 Re Pr \quad (22)$$

with  $Re = \frac{L}{\nu} \left( v_0^2 \cos^2(\pi x/d) \right)^{1/2} = v_0 L / (\sqrt{2} \nu)$ .

The amplitude  $\Delta z/L$  is shown in Fig. 6. When  $\Delta z/L$  is small, then the temperature field (21) is compatible with the boundary conditions in most of the volume. Deviations are expected only in layers of size  $\Delta z$  next to each boundary. Since  $\Delta z/L < 0.1$  for all points except one, we conclude that this solution provides us with a good description of

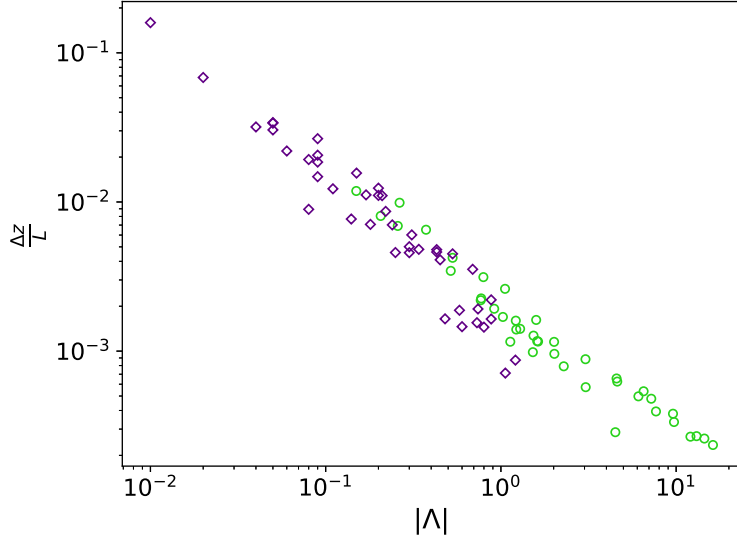


Figure 6.  $\frac{\Delta z}{L}$  as a function of  $|\Lambda|$ . The symbols are the same as in fig. 2.

the temperature field in the cell. Note that the analogous conclusion does not hold for the concentration field since the deformation amplitude of the isopycnics is larger by the factor  $Sc/Pr \approx 200$  and is at least comparable with the cell height for  $|\Lambda| < 1$ .

We now proceed with the solution (21) to compute the advective heat transport as

$$\langle v_z \theta \rangle = -\frac{v_0 d^2}{2\pi^2 \kappa} \partial_z \bar{T} \quad (23)$$

For a piecewise linear profile of mean temperature with a vertical gradient  $T_z$  in the bulk and a gradient of  $\Delta T_b/\lambda_T$  in thermal boundary layers of thickness  $\lambda_T$  and a temperature drop  $\Delta T_b$  across them, the gradients need to fulfill two conditions: The total temperature difference across the cell needs to be  $|\Delta T|$ ,

$$2\Delta T_b + T_z(L - 2\lambda_T) = |\Delta T| \quad (24)$$

and the heat flux through the boundary layers must equal the flux through the bulk, which leads with the help of eq. (23) to

$$-\kappa \frac{\Delta T_b}{\lambda_T} = -\kappa T_z - \frac{1}{2\pi^2} \frac{v_0^2 d^2}{\kappa} T_z. \quad (25)$$

One can eliminate  $\Delta T_b$  from these two equations to obtain

$$\frac{LT_z}{|\Delta T|} = \frac{1}{1 + \frac{2}{\pi^2} \frac{\lambda_T}{L} \left( Pr Re \frac{d}{L} \right)^2}. \quad (26)$$

If the actual finger thickness is equal to half the wavelength of the fastest growing mode in an infinite domain with temperature stratification  $T_z$ , then  $\frac{\pi}{d} \left( \frac{g\alpha T_z}{\kappa\nu} \right)^{-1/4} = \pi \frac{L}{d} |Ra_T|^{-1/4} \left( \frac{LT_z}{|\Delta T|} \right)^{-1/4} = \text{const.}$  This is different from the comparison in Fig. 5 because of the factor  $(LT_z/|\Delta T|)^{-1/4}$ . We need to know  $\lambda_T$  to compute  $LT_z/|\Delta T|$  from eq. (26), but we cannot measure  $\lambda_T$  directly. However,  $2\lambda_T/L \leq 1$  by definition which puts a lower bound on the possible values of  $LT_z/|\Delta T|$ . By evaluating eq. (26) with  $2\lambda_T/L = 1$ , one finds for most points (see fig. 7) that  $1 > LT_z/|\Delta T| > 0.2$  and hence  $1 > (LT_z/|\Delta T|)^{1/4} > 0.67$ . In the worst case, the points near  $\pi \frac{L}{d} |Ra_T|^{-1/4} = 1.4$  in Fig. 5 have  $\frac{\pi}{d} \left( \frac{g\alpha T_z}{\kappa\nu} \right)^{-1/4} = 1.4/0.67 = 2.1$  which is a factor of 2.3 above the value of 0.9 expected for most density ratios according to Fig. 4. This means that the observed finger thickness certainly agrees with the half wavelength of the fastest growing mode to better than a factor 2.3. If one accepts that the temperature gradient is nearly unaffected by finger convection and equal to  $-\Delta T/L$ , the agreement is to within a factor of  $1.4/0.9 \approx 1.5$ . Fig. 5 includes data for finger layers within staircases, so that the same conclusion holds for this class of fingers and if one assumes a thermal gradient of  $-\Delta T_f/L_f$  within the fingers. Considering the scatter in Fig. 7 it does not seem to be worthwhile to improve these factors. At any rate, it is difficult to find a better and trustworthy alternative to the gross overestimate of  $\lambda_T$  in Fig. 7. For example, one may attempt to model the diffusion in the temperature boundary layer, but the next section will point at limitations of this approach.

#### IV. SALINITY FLUX IN FINGERS

The simplest model for the boundary layers of the concentration field near one of the solid boundaries is that of ions diffusing with diffusivity  $D$  into a flow parallel to the boundary of velocity  $v$ . It takes the time  $d/v$  for the flow to travel horizontally across a finger so that the boundary layer thickness  $\lambda_c$  is proportional to  $(Dd/v)^{1/2}$ . Let the concentration drop across each boundary layer be  $\Delta c_b$ , so that the Sherwood number is given by  $Sh = L\Delta c_b/(\lambda_c\Delta c)$ . If there is no gradient left in the interior of the flow, then  $\Delta c_b = \Delta c/2$  and one obtains the classical formula  $Sh = L/(2\lambda_c)$ . This leads with  $\lambda_c \propto (Dd/v)^{1/2}$  to

$$Sh \propto (ScRe \frac{L}{d})^{1/2}. \quad (27)$$

This relation is verified in Fig. 8. The good agreement found in this figure does not prove that  $\Delta c/\Delta c_b = 2$ , but it shows that  $\Delta c/\Delta c_b$  varies little in dependence of the Rayleigh

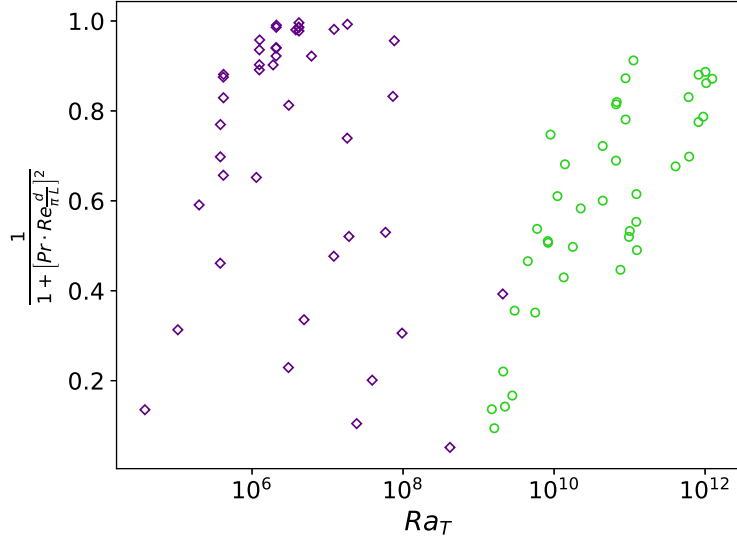


Figure 7. The smallest possible value of  $LT_z/|\Delta T|$  according to eq. (26) is given by  $1/[1 + [PrRed/(\pi L)]^2]$  and is shown as a function of  $|Ra_T|$ . The symbols are the same as in fig. 2.

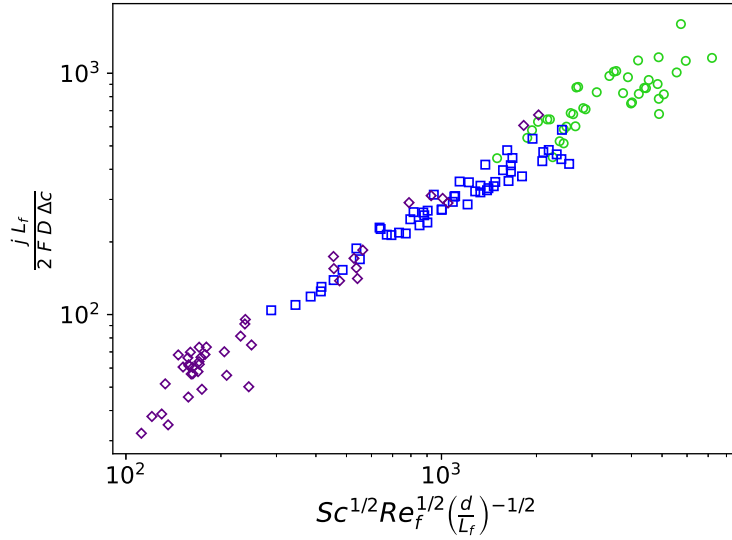


Figure 8.  $jL_f/(2FD\Delta c)$ , which is equal to  $Sh$  for fingers extending through the whole cell, as a function of  $(ScRe_f \frac{L_f}{d})^{1/2}$ . The symbols are the same as in fig. 2.

numbers. Salinity cannot diffuse from one finger to the neighboring finger during the time it takes to travel vertically across the cell at finger velocity<sup>7</sup>. Fingers therefore maintain the ion concentration they had when they started from one boundary until they hit the opposite boundary. Because of the top bottom symmetry of the system, the horizontally averaged

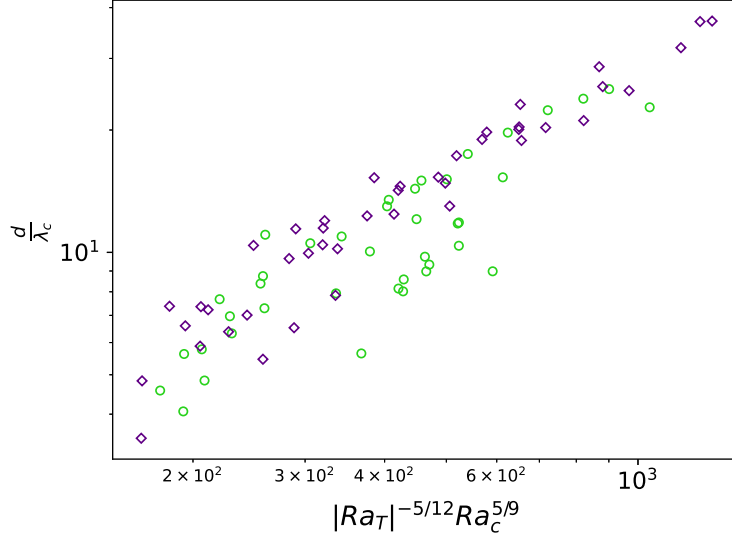


Figure 9.  $d/\lambda_c$  as a function of  $|Ra_T|^{-5/12} Ra_c^{5/9}$  which is the scaling for  $d/\lambda_c$  according to Ref. 7. The symbols are the same as in fig. 2.

concentration must therefore be  $c_0$  everywhere and the gradient  $\partial_z \bar{c}$  is zero in the bulk. Even though we cannot measure  $\Delta c_b$  directly, it is very plausible that  $\Delta c/\Delta c_b = 2$ .

The data points at low  $Ra_c$  in Fig. 2 obey simple scaling laws<sup>7</sup> for  $Re$ ,  $Sh$  and  $d/L$ . It is remarkable that these scaling laws exactly verify  $Sh \propto (Re \frac{L}{d})^{1/2}$  even though the exponents in these scalings were obtained from three independent fits to experimental data.

The picture of ions diffusing into a parallel flow to form a boundary layer is only useful if the boundary layer thickness  $\lambda_c$  is small compared with the horizontal distance over which the parallel flow exists, which is the finger width  $d$  in our application. If on the contrary  $d/\lambda_c \gg 1$  is not satisfied, one must expect significant ion diffusion into the stagnation points that exist on the boundaries at the edges of fingers and near which the flow is not parallel to the boundary. Fig. 9 shows that for  $\lambda_c$  computed from  $\lambda_c = L/(2Sh)$ , one indeed finds  $d/\lambda_c > 3.5$  for all data points and  $d/\lambda_c > 10$  for the majority of them.

The temperature boundary layer thickness  $\lambda_T$  is according to the same reasoning given by  $\lambda_T \propto (\kappa d/v)^{1/2}$  and  $\lambda_T = (Sc/Pr)^{1/2} \lambda_c \approx 14 \lambda_c$  so that  $d/\lambda_T < 1$  for many of the data points in our collection and  $\lambda_T \propto (\kappa d/v)^{1/2}$  must be a poor approximation of the true temperature boundary layer thickness. The model of a boundary layer created by diffusion into parallel shear flow is applicable to the salinity boundary layer and was already successfully used in some treatments of double diffusive convection<sup>8,18</sup> but it cannot be used throughout the full

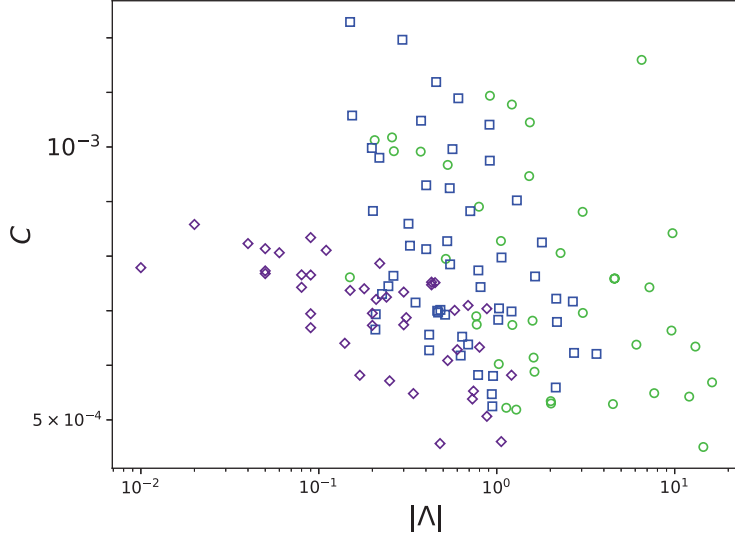


Figure 10.  $C = \beta j / [2F(g\kappa)^{1/3}(\beta\Delta c)^{4/3}]$  as a function of  $|\Lambda|$ . The symbols are the same as in fig. 2.

data set considered here for the temperature boundary layer.

Most previous experiments have confirmed the so called 4/3-law which states that  $j \propto \Delta c^{4/3}$ , or in non dimensional form including all control parameters,  $Sh \propto f(Pr, Sc, \Lambda) Ra_c^{1/3}$  with an undetermined function  $f$ . The exponent 1/3 is not the preferred value in the fits to the data obtained from the electrochemical cell, but it was already noted in Ref. 7 that the data are nearly indistinguishable from and hence compatible with the 4/3-law. The point that deserves attention here is not so much the exponent as the prefactor.

For better comparison with other experiments, let us consider the ion or salinity flux  $F_s$  in  $mol/(m^2s)$  which in the electrochemical cell can be determined from eq. (5) as  $F_s = j/(2F) = ShD\Delta c/L$  and seek the proportionality constant  $C$  in

$$\beta F_s = C(g\kappa)^{1/3}(\beta\Delta c)^{4/3}. \quad (28)$$

Values of  $C$  for finger convection in sea water can be found in Fig. 7 of Schmitt<sup>19</sup> who found that  $C$  decreases with  $|\Lambda|$  at small  $|\Lambda|$  and is approximately constant beyond  $|\Lambda| = 3$  with  $C \approx 0.05$ . A compilation of data appears in Fig. 5 of Taylor and Bucens<sup>20</sup> and shows compatible numbers. However, the values of  $C$  for the electrochemical cell shown in Fig. 10 lie in the interval  $5 \times 10^{-4} \lesssim C \lesssim 1.2 \times 10^{-3}$  and are therefore smaller by approximately a factor 100.

It is unlikely that such a large factor is due to minor changes in  $Pr$  and  $Sc$  with  $Pr = 7$

and  $Sc = 700$  for sea water and  $Pr = 9$  and  $Sc \approx 2000$  in our electrolyte. The ranges of Rayleigh numbers are also broadly similar in Fig. 7 of Schmitt<sup>19</sup> and Fig. 2. The potentially relevant difference that comes to mind is the nature of the finger tips. In the electrochemical cell, the fingers have one tip ending on a solid wall if they are part of a staircase, and both tips if they cross the entire cell. Older experiments started from two layers on top of each other, separated either by a steep step or a smooth profile of salinity and temperature, but in all cases, fingers were not in contact with a solid wall. It is plausible that this gives more freedom to the transport into and out of the fingers at their ends, even though the amplitude of the effect remains surprising.

An early experiment on double diffusive finger convection in salty water<sup>21</sup> measured the salinity flux between two layers, a warm fresh layer superimposed on cold salty water, with density ratios between 2 and 10. By lack of any other data, the author compared this salinity flux with the well investigated heat flux in thermal Rayleigh-Bénard convection and found a discrepancy by a factor of 10 to 40 between the two fluxes. Even though this study had to compare a salinity flux with a heat flux, it already indicated a large difference of fluxes depending on whether a solid wall is present or not.

Values of  $C$  can also be obtained from the 2D computations for  $Pr = 7$  and  $Sc = 700$  by Li and Yang<sup>11</sup> after rewriting eq. (28) as  $C = Ra_c^{-1/3} Sc^{-2/3} Pr^{1/3} Sh$ . These computations simulate fluid in a plane layer, but visualizations indicate that fingers are not necessarily in contact with one of the boundaries. One can compute from the tabulated results in the range  $10^9 \leq Ra_c \leq 10^{12}$  that  $0.0012 \leq C \leq 0.0015$  at  $|\Lambda| = 1$  and  $0.04 \leq C \leq 0.06$  at  $|\Lambda| = 3$ . These results are unusual in that  $C$  increases with  $|\Lambda|$ . The numerically obtained  $C$  lie in between the results in Schmitt<sup>19</sup> and Taylor and Bucens<sup>20</sup> and ours and do not provide us with a definitive answer on why the  $C$  in the electrochemical cell is so small.

A related set of results was obtained for the sugar/salt system. In these experiments in aqueous solution, sugar plays the role of the slowly diffusing and salt that of the rapidly diffusing component. The ratio of diffusivities is only 3 for this combination. Comparing again the flux law for the flux between two layers measured experimentally<sup>22</sup> with the flux computed numerically in a plane layer crossed by fingers, Radko and Stern<sup>23</sup> found good agreement indicating no difference between the dynamics of a bounded finger layer and fingers in a two layer system. The flux reducing effect of the solid wall seems to depend on parameters that remain to be identified.

## V. SALINITY FLUX IN STAIRCASES

The staircases were mostly omitted from the discussion so far because we do not have access to all their control parameters or their Sherwood number. We do not know the amplitude of the concentration and temperature differences that drive the convection in the fingers that are part of staircases.  $\Delta T_f$  enters Fig. 5 only to the power 1/4 so that the figure is rather insensitive to the correct value of  $\Delta T_f$  and it is innocuous to compare all types of fingers in this figure.

There are two other relations which actually inform us about the correct concentration difference for fingers in staircases. The first observation concerns eq. (27). Fig. 8 was drawn with a  $\Delta c$  in the definition of  $Sh$  which is by definition the correct choice for fingers crossing the whole cell, but as can be seen in the figure, it is also the correct choice for fingers within staircases! In the derivation of eq. (27),  $\Delta c$  stands for twice the concentration drop across the boundary layer. According to Fig. 8, this quantity is identical to  $\Delta c$ , the concentration difference between the two electrodes, for both fingers in staircases and fingers spanning the whole cell. This then implies that the horizontally averaged concentration of ions outside the boundary layers is the same in both types of fingers. This means that the concentration contrast between rising and sinking fingers must always be  $\Delta c$  to obtain the correct horizontal average. A finger falling down from the top plate must meet with fingers carrying the ion concentration of the bottom plate to yield  $c_0$  in the horizontal average. This implies that a blob of fluid leaving for example the bottom plate with a low ion concentration rises through both the lower finger layer and the central convecting layer without gaining ions so that it arrives at the bottom edge of the top layer with still the same ion concentration. This applies a concentration difference of a full  $\Delta c$  to the top layer. The symmetric reasoning holds for a blob leaving the top plate passing unscathed both the top layer and the central layer so that again there is a concentration difference of  $\Delta c$  applied to the bottom layer, too. It was expected that fluid travels through the finger layers without a change in ion concentration<sup>7</sup>, but it is more surprising to see that the central layer does not mix the fluid and does not equalize the concentration in its interior. For this to be possible, the blobs which have traversed the central layer and impinge on the edge of a finger layer must be quickly absorbed by that layer before they get entrained in the circulation of the central convection roll which would inevitably lead to mixing. The interface between finger

layers and convection rolls must be very permeable.

This picture is supported by the behaviour of the proportionality constant  $C$  in the 4/3-law. The expression for  $C$  in eq. (28) also contains a  $\Delta c$ , which is identical for all classes of fingers in Fig. 10. This figure shows that both fingers extending through the whole cell and fingers in staircases obey the 4/3-law with the same proportionality constant if and only if it is again assumed that the concentration difference across every finger layer is  $\Delta c$ .

These observations motivate the definition of  $Ra_{c,f}$  in eq. (8) with  $\Delta c_f = \Delta c$ . The relations represented in Figs. 8 and 10 are independent of the temperature field so that they probe the correct  $\Delta c_f$  independently of the correct choice for  $\Delta T_f$ . The temperature difference  $\Delta T_f$  in the definition of  $Ra_{T,f}$  is chosen to be  $\Delta T_f = \Delta T/2$  because this leads to the best fit in Fig. 3. It is possible that because of the more rapid diffusion of heat, temperature differences in the central convecting layer are erased while concentration differences remain, so that half of the total temperature drop occurs over each finger layer. However,  $Ra_{T,f}$  only occurs in Figs. 3 and 5, raised to the power 1/3 or 1/4, so that the data do not discriminate well between different choices of  $\Delta T_f$ .

## VI. CONCLUSION

Measurements on double diffusive finger convection in an electrochemical cell were analyzed in this paper and compared with results obtained from other double diffusive systems. A major motivation for this comparison is that fingers in the electrochemical cell at the control parameters investigated so far are always limited in their extent by a solid boundary. This is different from other experimental systems in which fingers are detached from solid boundaries.

A generalization of the scaling law<sup>7</sup> found for finger thickness at  $Ra_c < 10^{12}$  to all fingers on which measurements are available in the electrochemical cell leads to a satisfactory fit to all data, including to those for fingers within staircases. However, there is no ab initio theory to derive this scaling law. Past experiments and simulations indicate that finger widths agree well with half the wavelength of the fastest growing mode found in linear stability analysis. There is no theory either for why the flow in the saturated state should have the same finger size as during a growth phase, but it is intuitive to assume so. For the double diffusive convection in the electrochemical cell, the observed finger width and the width of the fastest

growing mode agree to within a factor 1.5 if one assumes that the thermal gradient along the fingers is the average thermal gradient imposed by boundary conditions. The actual gradient within the fingers might be less, but the agreement must still be to within a factor 2.3 or better.

The salinity transport conforms with the 4/3-law, but the proportionality factor appearing in this law is much smaller in the experiments analyzed here than in previous experiments. A plausible explanation for this discrepancy is precisely that fingers were surrounded by fluid from all sides in the older experiments, whereas at least one tip of every finger borders a solid wall in the experiments in the electrochemical cell. The presence of a wall certainly restricts the dynamics and reduces the transport through the finger tips, but it is noteworthy that this reduction is by two orders of magnitude.

The transport through finger tips in the absence of a solid boundary is so efficient that it prevents overturning layers sandwiched between two finger layers in staircases to mix the fluid in their interior well enough to annihilate concentration gradients. Plumes colliding with finger tips seem to be siphoned into the finger layer before they lose much concentration contrast with their environment. Some mixing in the overturning layer must of course occur, but it is too small to be detectable in staircases that contain just one overturning layer. The implications for staircases with many more layers remain to be explored.

Data sharing is not applicable to this article as no new data were created or analyzed in this study.

## ACKNOWLEDGMENTS

This work was supported by the DFG under the grant Ti243/15 as part of the priority programme "Reconstructing the Deep Dynamics of Planet Earth over Geologic Time".

## REFERENCES

- <sup>1</sup>J. S. Turner, "Double-diffusive phenomena," *Ann. Rev. Fluid Mech.* **6**, 37–56 (1974).
- <sup>2</sup>J. S. Turner, "Multicomponent convection," *Ann. Rev. Fluid Mech.* **17**, 11–44 (1985).
- <sup>3</sup>T. Radko, "What determines the thickness of layers in a thermohaline staircase?" *J. Fluid Mech.* **523**, 79–98 (2005).

- <sup>4</sup>A. Tilgner, “Experiments on double diffusive convection,” *Comptes Rendus. Physique* (2024), 10.5802/crphys.194.
- <sup>5</sup>R. Krishnamurti, “Double-diffusive transport in laboratory thermohaline staircases,” *J. Fluid Mech.* **483**, 287–314 (2003).
- <sup>6</sup>R. Krishnamurti, “Heat, salt and momentum transfer in a laboratory thermohaline staircase,” *J. Fluid Mech.* **638**, 491–506 (2009).
- <sup>7</sup>E. Hage and A. Tilgner, “High Rayleigh number convection with double diffusive fingers,” *Phys. Fluids* **22**, 076603 (2010).
- <sup>8</sup>Y. Yang, E. P. van der Poel, R. Ostillá-Mónico, C. Sun, R. Verzicco, S. Grossmann, and D. Lohse, “Salinity transfer in bounded double diffusive convection,” *Journal of Fluid Mechanics* **768**, 476–491 (2015).
- <sup>9</sup>Y. Yang, R. Verzicco, and D. Lohse, “Vertically bounded double diffusive convection in the finger regime: Comparing no-slip versus free-slip boundary conditions,” *Phys. Rev. Lett.* **117**, 184501 (2016).
- <sup>10</sup>Y. Yang, W. Chen, R. Verzicco, and D. Lohse, “Multiple states and transport properties of double-diffusive convection turbulence,” *Proc. Nat. Acad. Sci.* **117**, 14676–14681 (2020).
- <sup>11</sup>J. Li and Y. Yang, “On the wall-bounded model of fingering double diffusive convection,” *Journal of Fluid Mechanics* **973**, A37 (2023).
- <sup>12</sup>A. Mani and K. M. Wang, “Electroconvection near electrochemical interfaces: Experiments, modeling, and computation,” *Annual Review of Fluid Mechanics* **52**, 509–529 (2020).
- <sup>13</sup>M. Kellner and A. Tilgner, “Transition to finger convection in double-diffusive convection,” *Phys. Fluids* **26**, 094103 (2014).
- <sup>14</sup>A. Rosenthal, K. Lüdemann, and A. Tilgner, “Staircase formation in unstably stratified double diffusive finger convection,” *Phys. Fluids* **34**, 116605 (2022).
- <sup>15</sup>R. J. Goldstein, H. D. Chiang, and D. L. See, “High-Rayleigh-number convection in a horizontal enclosure,” *J. Fluid Mech.* **213**, 111–126 (1990).
- <sup>16</sup>R. W. Schmitt, “The growth rate of super-critical salt fingers,” *Deep-Sea Research* **26A**, 23–40 (1978).
- <sup>17</sup>R. W. Schmitt, “Thermohaline convection at density ratios below one: A new regime for salt fingers,” *J. Mar. Res.* **69**, 779–795 (2011).
- <sup>18</sup>T. Tassin, T. Gastine, and A. Fournier, “Fingering convection in a spherical shell,” *Journal*

- of Fluid Mechanics **988**, A18 (2024).
- <sup>19</sup>R. W. Schmitt, “Flux measurements on salt fingers at an interface,” *J. Mar. Res.* **37**, 419–436 (1979).
- <sup>20</sup>J. Taylor and P. Bucens, “Laboratory experiments on the structure of salt fingers,” *Deep-Sea Research* **36**, 1675–1704 (1989).
- <sup>21</sup>J. S. Turner, “Salt fingers across a density interface,” *Deep-Sea Res.* **14**, 499–611 (1967).
- <sup>22</sup>J. R. Taylor and G. Veronis, “Experiments on double-diffusive sugar-salt fingers at high stability ratio,” *Journal of Fluid Mechanics* **321**, 315–333 (1996).
- <sup>23</sup>T. Radko and M. Stern, “Finite-amplitude salt fingers in a vertically bounded layer,” *J. Fluid Mech.* **425**, 133–160 (2000).

$\nu, \kappa, D$	diffusion constants for momentum, temperature and salinity	$m^2 s^{-1}$
$g$	gravitational acceleration	$ms^{-2}$
$\alpha$	thermal expansion coefficient	$K^{-1}$
$\beta$	compositional expansion coefficient	$mol^{-1}$
$L$	height of the cell	$m$
$L_f$	height of a finger layer	$m$
$d$	finger thickness	$m$
$\lambda_c$	thickness of compositional boundary layer	$m$
$T$	temperature	$K$
$\theta$	difference between the temperature and the linear conduction profile	$K$
$\Delta T$	temperature difference between bottom and top of the cell	$K$
$\Delta T_f$	temperature difference between bottom and top of a finger layer	$K$
$c$	concentration	$mol/m^3$
$s$	difference between the concentration and the linear diffusion profile	$mol/m^3$
$\Delta c$	concentration difference between top and bottom of the cell	$mol/m^3$
$\Delta c_f$	concentration difference between top and bottom of a finger layer	$mol/m^3$
$c_0$	concentration averaged over the cell	$mol/m^3$
$F$	Faraday constant	$As mol^{-1}$
$F_s$	salinity flux	$mol m^{-2} s^{-1}$
$j$	current density	$Am^{-2}$
$Sh$	Sherwood number	
$\Lambda$	density ratio	
$Ra_T, Ra_c, Re$	thermal Rayleigh, compositional Rayleigh and Reynolds numbers based on the height of the cell	
$Ra_{T,f}, Ra_{c,f}, Re_f$	thermal Rayleigh, compositional Rayleigh and Reynolds numbers based on the height of a finger layer	
$Pr$	Prandtl number	
$Sc$	Schmidt number	

Table I. Most symbols occur only locally in this paper and are defined where they are used. Symbols that occur throughout the paper are collected in this table. The third column is empty for non dimensional variables and contains the units otherwise.